bioRxiv preprint doi: https://doi.org/10.1101/2020.03.24.005561; this version posted March 27, 2020. The copyright holder for this preprint (which was not certified by peer review) is the author/funder, who has granted bioRxiv a license to display the preprint in perpetuity. It is made available under aCC-BY-NC-ND 4.0 International license.

Computational simulations reveal the binding dynamics between human ACE2 and the receptor binding domain of SARS-CoV-2 spike protein

Cecylia S. Lupala[a], Xuanxuan Li[b,a], Jian Lei[c], Hong Chen[e], Jianxun Qi[f], Haiguang Liu[a,d,*], Xiao-dong Su[e,*]

[a]Complex Systems Division, Beijing Computational Science Research Center, Haidian, Beijing 100193, People's Republic of China

[b]Engingeering Physics Department, Tsinghua University, Haidian, Beijing 100084, People's Republic of China

[c]State Key Laboratory of Biotherapy and Cancer Center, National Clinical Research Center for Geriatrics, West China Hospital, Sichuan University, Chengdu, Sichuan 610041, People's Republic of China

[d]Physics Department, Beijing Normal University, Haidian, Beijing 100875, People's Republic of China

[e]School of Life Sciences, State Key Laboratory of Protein and Plant Gene Research and Biomedical Pioneering Innovation Center (BIOPIC), Peking University, Beijing 100871, People's Republic of China

[f]CAS Key Laboratory of Pathogenic Microbiology and Immunology, Institute of Microbiology, Chinese Academy of Sciences, Beijing, 100101, People's Republic of China

Keywords: SARS-CoV-2, Spike protein, RBD, ACE2, Molecular Dynamics

*Corresponding authors: Haiguang Liu, hgliu@csrc.ac.cn and
Xiao-dong Su, xdsu@pku.edu.cn

bioRxiv preprint doi: https://doi.org/10.1101/2020.03.24.005561; this version posted March 27, 2020. The copyright holder for this preprint (which was not certified by peer review) is the author/funder, who has granted bioRxiv a license to display the preprint in perpetuity. It is made available under aCC-BY-NC-ND 4.0 International license.

Abstract

A novel coronavirus (the SARS-CoV-2) has been identified in January 2020 as the causal pathogen for COVID-19 pneumonia, an outbreak started near the end of 2019 in Wuhan, China. The SARS-CoV-2 was found to be closely related to the SARS-CoV, based on the genomic analysis. The Angiotensin converting enzyme 2 protein (ACE2) utilized by the SARS-CoV as a receptor was found to facilitate the infection of SARS-CoV-2 as well, initiated by the binding of the spike protein to the human ACE2. Using homology modeling and molecular dynamics (MD) simulation methods, we report here the detailed structure of the ACE2 in complex with the receptor binding domain (RBD) of the SARS-CoV-2 spike protein. The predicted model is highly consistent with the experimentally determined complex structures. Plausible binding modes between human ACE2 and the RBD were revealed from all-atom MD simulations. The simulation data further revealed critical residues at the complex interface and provided more details about the interactions between the SARS-CoV-2 RBD and human ACE2. Two mutants mimicking rat ACE2 were modeled to study the mutation effects on RBD binding to ACE2. The simulations showed that the N-terminal helix and the K353 of the human ACE2 alter the binding modes of the CoV2-RBD to the ACE2.

Introduction

The outbreak of a new type of severe pneumonia COVID-19 started in December 2019 [1] has been going on world-wide, and caused over 15,000 fatalities, infected more than 350,000 individuals globally. Although the earlier infected cases were mainly found in China before March, 2020, particularly in Hubei Province, the confirmed COVID-19 cases have been reported in more than 160 countries or territories by the end of March, 2020, and still increasing rapidly. One urgent desire in coping with this global crisis is to develop or discover drugs that can treat the diseases caused by the novel coronavirus, the SARS-CoV-2 (also known as 2019-nCoV)[2]. According to the genome comparative studies, the SARS-CoV-2 belongs to the genus beta-coronavirus, with nucleotide sequence identity of about 96% compared to the closest bat coronavirus RaTG13, about 89% compared to two other bat SARS-like viruses (Bat-SL-CoVZC45 & Bat-SL-CoVZXC21), and 79% compared to

bioRxiv preprint doi: https://doi.org/10.1101/2020.03.24.005561; this version posted March 27, 2020. The copyright holder for this preprint (which was not certified by peer review) is the author/funder, who has granted bioRxiv a license to display the preprint in perpetuity. It is made available under aCC-BY-NC-ND 4.0 International license.

the SARS-CoV [3,4]. Furthermore, the SARS-CoV-2 spike protein has a protein sequence identity of 73% for the receptor binding domain (RBD) with the SARS-CoV RBD (denoted as SARS-RBD in the following). The SARS-CoV and SARS-CoV-2 both utilize the human Angiotensin converting enzyme 2 protein (ACE2) to initiate the spike protein binding and facilitate the fusion to host cells [5–9]. The 193-residue RBD of the SARS-CoV spike protein has been found to be sufficient to bind the human ACE2 [6]. Based on this fact, the RBD of SARS-CoV-2 becomes a critical protein target for drug development to treat the COVID-19. When this study was started, neither the crystal structure of the SARS-CoV-2 spike protein nor the RBD segment were determined, so the homology modeling approach was applied to construct the model of the SARS-CoV-2 spike RBD in complex with the human ACE2 binding domain (denoted as CoV2-RBD/ACE2 in the following). Similar approach has been applied to predict the complex structure and estimate the binding energies [3]. Because of the high sequence similarity between CoV2-RBD and SARS-RBD, the predicted structure was found to be highly consistent with the resolved crystal structures [10] (see another crystal structure at http://nmdc.cn/nCoV entry:NMDCS0000001, PDBID: 6LZG). These structures laid the foundation for the dynamics investigation of the CoV2-RBD/ACE2 complex using computational simulation method. The predicted CoV2-RBD/ACE2 model was subjected to all-atom molecular dynamics (MD) simulations to study the binding interactions.

Although the crystal structure and the predicted model of the CoV2-RBD/ACE2 complex provide important information about the binding interactions at the molecular interfaces, MD simulations can extend the knowledge to a dynamics regime in a fully solvated environment. The importance of the ACE2 residues was investigated by simulating the complexes with ACE2 mutants, in which partial dissociation from the ACE2 was observed within 500 ns simulations. The control simulations of the SARS-RBD/ACE2 complexes allowed the detailed comparison in receptor binding for the two different types of viruses. The results showed that the wild type CoV2-RBD/ACE2 complex is stable in 500 ns simulations, especially in the well-defined binding interface. On the other hand, the mutations on the helix-1 or K353 of the ACE2 can alter the binding, revealing new binding poses with reduced contacts compared to those in the crystal structures. The analysis of the interaction energy showed that the binding is enhanced by adjusting conformations to form more favorable interactions as the simulation progressed, consistent with the increased hydrogen bonding patterns. Furthermore, the analysis also showed that SARS-RBD and

bioRxiv preprint doi: https://doi.org/10.1101/2020.03.24.005561; this version posted March 27, 2020. The copyright holder for this preprint (which was not certified by peer review) is the author/funder, who has granted bioRxiv a license to display the preprint in perpetuity. It is made available under aCC-BY-NC-ND 4.0 International license.

CoV2-RBD have comparable binding affinities to the ACE2, with the former slightly stronger than the latter. The dynamic information obtained by this study shall be useful in understanding SARS-CoV-2 host interaction and for designing inhibitors to block CoV2-RBD binding.

Methods

The computer model of the SARS-CoV-2 spike RBD in complex with human ACE2

The spike RBD of SARS-CoV-2 (GenBank: MN908947 [2]) comprises Cys336-Gly526 residues according to the sequence homology analysis with SARS-CoV spike RBD. The predicted three-dimensional structure model of these residues was obtained with the SWISS-MODEL server [11]. This predicted SARS-CoV-2 RBD model was subsequently superimposed into the X-ray structure of SARS-CoV RBD in complex with human ACE2 (PDB code:2AJF, Chain D [7]). Finally, the computer model of SARS-CoV-2 RBD with human ACE2 (CoV2-RBD/ACE2) was obtained for further simulations and analysis.

Mutant preparation

Based on the analysis of the predicted model, sequence alignment, and literature survey, two other systems containing mutations in the human ACE2 were prepared and subject to MD simulation studies. The mutant construct is based on the fact that Rat ACE2 markedly diminishes interactions with SARS spike protein [12], and it was proposed that the rat ACE2 likely has reduced binding affinity to the CoV2-RBD [13]. To investigate the roles of critical residues on the ACE2, we created two mutants of the human ACE2 (see Table 1): (1) mutant *mut_h1*, with the ACE2 N-terminal (residue 19-40) mutated to the residues of rat ACE2; and (2) mutant *K353H*, in which the highly conserved K353 was mutated to histidine (the corresponding amino acid in rat and mouse ACE2 proteins). To focus on the impact of these two binding sites, the rest of the ACE2 were kept to be the same as human ACE2.

Molecular Dynamics Simulation and Analysis

The predicted model of CoV2-RBD/ACE2 complex was used as the starting models for MD simulations. The spike protein RBD domain is composed of 180 residues (323-502), while the ACE2 protein contains 597 residues (19-615) from the N-terminal domain. The simulation parameterization and equilibration were prepared for complex structures including

bioRxiv preprint doi: https://doi.org/10.1101/2020.03.24.005561; this version posted March 27, 2020. The copyright holder for this preprint (which was not certified by peer review) is the author/funder, who has granted bioRxiv a license to display the preprint in perpetuity. It is made available under aCC-BY-NC-ND 4.0 International license.

the mutant systems, using the CHARMM-GUI webserver [14]. Each system was solvated in TIP3P water and sodium chloride ions to neutralize the systems to a salt concentration of 150 mM. Approximately, each system was composed of about 220,000 atoms that were parametrized with the CHARMM36 force field [15].

After energy minimization using the steepest descent algorithm, each system was equilibrated at human body temperature 310.15 K, which was maintained by Nose-Hoover scheme with 1.0 ps coupling constant in the NVT ensemble (constant volume and temperature) for 125.0 ps under periodic boundary conditions with harmonic restraint forces applied to the complex molecules (400 kJ mol^{-1} nm^{-2} on backbone and 40 kJ mol^{-1} nm^{-2} on the side chains) [16,17]. In the subsequent step, the harmonic restraints forces were removed and the NPT ensemble were simulated at one atmosphere pressure (10^5 Pa) and body temperature. The pressure was maintained by isotropic Parrinello-Rahman barostat at 1.0 bar [18], with a compressibility of 4.5×10^{-5} bar^{-1} and coupling time constant of 5.0 ps. The simulation trajectories were propagated to 500 nanoseconds using the GROMACS 5.1.2 package [19].

Three independent trajectories starting from random velocities based on Maxwell distributions were simulated for both CoV2-RBD/ACE2 and SARS-RBD/ACE2 complex systems in their wild types. In all simulations, a time step of 2.0 fs was used and the PME (particle mesh Ewald) [20] was applied for long-range electrostatic interactions. The van der Waals interactions were evaluated within the distance cutoff of 12.0 Å. Hydrogen atoms were constrained using the LINCS algorithm [21].

The human ACE2 mutants in complex with CoV2-RBD were constructed as described previously. Each mutant complex model was simulated in two independent trajectories. Furthermore, as the crystal structure of the CoV2-RBD/ACE2 complex became available, two additional simulations were carried out using the crystal structure as the starting model to cross-validate the simulation results based on the homology model. Each trajectory was propagated to 500 ns by following the same protocol as the wild type CoV2-RBD/ACE2 complex simulations.

Analyses were carried out with tools in GROMACS (such as rmsd, rmsf, energy, and pairdist) to examine the system properties, such as the overall stability, local residue and general structure fluctuations through the simulations. The *g_mmpbsa* program [22] was applied

bioRxiv preprint doi: https://doi.org/10.1101/2020.03.24.005561; this version posted March 27, 2020. The copyright holder for this preprint (which was not certified by peer review) is the author/funder, who has granted bioRxiv a license to display the preprint in perpetuity. It is made available under aCC-BY-NC-ND 4.0 International license.

to extract the molecular mechanics energy E_{MM} (Lennard Jones and electrostatic interactions) between ACE2 and the RBD of spike proteins. VMD and Chimera were applied to analyze the hydrogen bonds, molecular binding interface, water distributions, visualization and rending model images [23,24].

Results

The homology structure of the CoV2-RBD/ACE2 was compared to the SARS-RBD/ACE2 crystal structure and the newly resolved crystal structure of the CoV2-RBD/ACE2. The results indicated that the homology model is accurate, especially at the binding interface. The MD simulations further refined the side chain orientations to improve the model quality. The simulation data revealed the stable binding between the CoV2-RBD and the ACE2, in spite of the conformational changes of the ACE2. The relative movement between the CoV2-RBD and the ACE2 mainly exhibited as a swinging motion pivoted at the binding interface. Simulations also revealed the roles of water molecules in the binding of the RBD to the ACE2 receptor. The MD simulation of complex with ACE2 mutants suggested that mutation to the ACE2 helix-1 and the K353 can alter the binding modes and binding affinity.

1. Homology modeling and comparison to the SARS-RBD/ACE2 complex

The predicted CoV2-RBD/ACE2 complex structure is highly similar to the SARS-RBD/ACE2, as shown in Figure 1. The RBD domain has an RMSD of 0.99 Å for the aligned residues (1.53 Å for all 174 residue pairs), indicating that the homology model of the CoV2-RBD is in good agreement with the SARS-RBD. For ACE2 residues near the binding interface (within 4.0 Å of the RBD), the RMSD is smaller than 0.43 Å compared to the SARS-RBD/ACE2 complex. The superposed structures revealed that the RBD/ACE2 interfaces are almost identical in two complexes(Figure 1c).

In a retrospective comparison, the predicted complex structure was superposed to the newly resolved crystal models (see Figure 2d for a detailed comparison at the interface). The results indicated that the homology model is very accurate, especially for the binding interface. The residues near the CoV2-RBD/ACE2 interface (defined as the combined set of ACE2 residues within 4.0 Å of RBD and the RBD residues within 4.0 Å of the ACE2) exhibited a difference of 0.43 Å RMSD, which is comparable to the difference between the

bioRxiv preprint doi: https://doi.org/10.1101/2020.03.24.005561; this version posted March 27, 2020. The copyright holder for this preprint (which was not certified by peer review) is the author/funder, who has granted bioRxiv a license to display the preprint in perpetuity. It is made available under aCC-BY-NC-ND 4.0 International license.

two independently reported crystal models (an RMSD of 0.25 Å for the same comparison). The RMSD is about 0.77 Å for residues in an extended region within 10.0 Å of the binding interface. The RBD domain of the spike protein showed an overall RMSD values less than 1.5 Å, and the ACE2 domain with an RMSD about 2.0 Å between the predicted model and the crystal structures.

2. The conformational changes of the ACE2 and the CoV2-RBD

The structural comparison revealed that MD simulations mainly sampled the structures in the conformational space near the starting model. The RMSD with respect to the starting model indicated that the sampled structures were mostly 2.5 Å to 5.0 Å compared to the starting model (Figure 3a). The largest contribution to the conformational changes in CoV2-RBD is from the loop regions, indicated by the peaks shown in the fluctuation plots (Figure 3b). The residues with well-defined secondary structures (mainly β-strands) exhibited very small conformational changes (the RMSD is about 1.0 Å including side chain atoms), while the loop regions have RMSD values between 3.7 Å to 5.4 Å. This is consistent with the residue fluctuations measured with the RMSF (root-mean-square-fluctuation) for the RBD subunit (Figure 3b). For the ACE2 receptor domain, the major conformational change is the opening/closing of the enzymatic active site, which is remote from the RBD binding interface (see Video 1). The CoV2-RBD remained bound to human ACE2, even though substantial conformational changes occurred to the ACE2 and the loop region of the RBD. This observation implies that the binding of CoV2-RBD to the ACE2 is very stable, similar with the case of the SARS-RBD that binds to both open and closed forms of human ACE2 [7,25].

Based on the structural similarity, a clustering analysis was carried out to identify the most populated structures, from which the representative model for each trajectory was selected (Figure 3). The CoV2-RBD/ACE2 interfaces were highlighted using blue/red colors with stick representations. The RMSD of structures in the simulations were calculated with respect to the these representative models, in order to assess the model convergence and coverage of the simulated conformations (Figure 3a, right panels). The RMSD values indicated that a large portions of the structures sampled by the MD simulations are similar to the representative model (Figure 3a, for trajectory 1, see supplementary materials for the other trajectories). Furthermore, as the simulation progressed, the conformations converged to the representative model obtained from this trajectory. This indicates that the selected

bioRxiv preprint doi: https://doi.org/10.1101/2020.03.24.005561; this version posted March 27, 2020. The copyright holder for this preprint (which was not certified by peer review) is the author/funder, who has granted bioRxiv a license to display the preprint in perpetuity. It is made available under aCC-BY-NC-ND 4.0 International license.

structure is plausible and stable. The representative structures for the other two trajectories showed smaller deviations compared to the predicted model (Figure 2b and 2c).

In three simulations of the CoV2-RBD/ACE2 systems, the binding interface was highly stable, exhibiting very small conformational changes, especially for the interfacing residues of the ACE2 protein. The RMSD for the residues at the RBD binding interface is 0.85Å (+/-0.13Å) on average. Side chain atom positions were refined to form more favorable interactions (Figure 2d). One outstanding example is the K31 side-chain, which pointed in the wrong orientation in the predicted structure, was quickly refined to the correct orientation, consistent with the crystal structure (right panel of Figure 2d).

In terms of collective conformational changes, the CoV2-RBD/ACE2 complex showed two interesting movements: (1) the loop (L_{67}) between β_6 and β_7 (residues between S477 and G485 in particular) of CoV2-RBD was found to expand its interactions with the N-terminal helix (the helix-1) of the ACE2 (Figure 2a), while it pointed away from the helix-1 in the predicted and the crystal structures (Figure 2d, left); (2) a tilting movement of the RBD relative to the ACE2 was observed, which can be depicted as a swinging motion with the binding interface as the pivot (see Figure 4 for an illustration). In both predicted and the crystal structures of the CoV2-RBD/ACE2 complex, the L_{67} does not form close contacts with the ACE2. The analysis of the crystal packing revealed that this loop participated in the interaction with another asymmetric unit (see Supplemental Information). Interestingly, the simulation data suggested that the L_{67} could move towards the ACE2 and form contacts with the helix-1. This can potentially enhance the binding, as reflected in the change of interaction energies. In the crystal structure, the C480 and C488 of the RBD are cross-linked via a disulfide bond that reduces the flexibility of the L_{67} region, limiting its access to the ACE2. On the other hand, it has been reported that the binding of SARS-RBD to ACE2 is insensitive to the redox states of the cysteines to a high extend [26]. Based on the simulation results, we hypothesize that the reduced form of C480 and C488 can also exist during the virus invasion to host cells, and the reduced cysteines can potentially enhance the binding to ACE2. In the other two simulation trajectories, we found that the L_{67} remained in conformations similar to that in the crystal structure and the cysteines (C480 and C488) were close enough for disulfide bond formation.

bioRxiv preprint doi: https://doi.org/10.1101/2020.03.24.005561; this version posted March 27, 2020. The copyright holder for this preprint (which was not certified by peer review) is the author/funder, who has granted bioRxiv a license to display the preprint in perpetuity. It is made available under aCC-BY-NC-ND 4.0 International license.

3. Simulations revealed detailed binding interface interactions between the CoV2-RBD and the ACE2

By examining the binding interface of CoV2-RBD and the ACE2, we found the polar and charged residues account for a large fraction, therefore the electrostatic interactions play critical roles for the complex formation. Based on the distances between the two proteins, the key residues at the binding interface were identified and summarized in Table 2 for the three representative models (see Figure 2). Majority of these residues are conserved for these three models, except that the model#1 (Figure 2a) has additional contacts to the ACE2 from residues in the L_{67} region (highlighted with green color in Table 2). As shown in Figure 2, the L_{67} remained in the starting position for the other two representative models (Figure 2b,c). The same simulations were carried out for the SARS-RBD/ACE2 complex, serving as a comparative system. Interestingly, the SARS-RBD counterpart of the L_{67} in CoV2-RBD did not form close contacts with the ACE2 in three simulations. It is worthwhile to mention that the sequence identity between CoV2-RBD and SARS-RBD is low in this loop region, suggesting the loop region might be partially responsible for the difference in the receptor binding.

The hydrogen bonds between the CoV2-RBD and ACE2 were extracted using VMD program with default criteria (D-A distance cutoff=3.0 Å and D-H-A angle cutoff=20 degrees, where D,A,H are Donor atom, Acceptor atom, and the Hydrogen atom linked to the Donor atom). The numbers of hydrogen bonds are summarized in Figure 5 for the simulation trajectory#1. Because of the stringent criteria for hydrogen bonds, the numbers are smaller compared to the reported values in other studies. For a larger distance cutoff of 3.9Å, there are about 8.3 hydrogen bonds on average (Figure 5b). We observed that the number of hydrogen bonds fluctuated over time, and exhibiting an overall increasing trend indicated by the fitted lines (Figure 5). Similar trends were observed in the other simulations, suggesting that the binding became stronger as the simulation progressed. Based on the statistics of three simulation trajectories, the CoV2-RBD/ACE2 complex has 2.7 hydrogen bonds between the subunits on average with stringent criteria. In comparison, the SARS-RBD/ACE2 has 3.2 hydrogen bonds on average (see Supplementary Information). The statistics of hydrogen bonds suggest a slightly weaker binding between the CoV2-RBD and the ACE2, relative to the SARS-RBD/ACE2 complex.

bioRxiv preprint doi: https://doi.org/10.1101/2020.03.24.005561; this version posted March 27, 2020. The copyright holder for this preprint (which was not certified by peer review) is the author/funder, who has granted bioRxiv a license to display the preprint in perpetuity. It is made available under aCC-BY-NC-ND 4.0 International license.

It is also noteworthy to point out the important roles of water molecules at the complex interface for CoV2-RBD/ACE2 complex. At any instant time, there are approximately 15 water molecules at the binding interface, simultaneously located within 2.5 Å of both the CoV2-RBD and the ACE2 (Figure 6). These water molecules can function as bridges by forming hydrogen bonds with the residues from the RBD or the ACE2. The dwelling time of water molecules at the interface can be a few nanoseconds, as revealed by the MD simulations. This results is also consistent with the crystal structure, which has 12 water molecules at the interface (Figure 6c). These discoveries emphasize the role of the water molecules, which desires detailed quantification to understand the interactions between the RBD and the ACE2.

4. Simulation of the human ACE2 mutants uncovers new binding modes

It has been demonstrated that the ACE2 from several mammalian species possess high sequence similarities, yet their binding to the SARS-RBD differs significantly. In particular, the binding of SARS-RBD to the rat ACE2 is much weaker as discovered in experiments [12]. Inspired by these information, two mutants of the CoV2-RBD/ACE2 were constructed: (1) *ACE2-mut-h1* by mutating N-terminal helix-1 to that of the rat ACE2; (2) *ACE2-K353H* by mutating K353 to Histidine (the amino acid in wild type Rat ACE2). Two 500ns MD simulations were carried out for each mutant system. The simulation showed that the mutations in *ACE2-mut-h1* reduced the interaction between the CoV2-RBD and the helix-1, and the *ACE2-K353H* showed weaker binding between the CoV2-RBD and the β-hairpin centered at the H353. Using the clustering analysis, the representative structures were identified from each simulation trajectory (Figure 7). Although the overall topology is very similar to the wild type complex structure, there are pronounced differences. For the *ACE2-mut-h1* system, the CoV2-RBD tilted further away from the ACE12 helix-1 in one simulation (Figure 7a); and the CoV2-RBD lost its contact with helix-13 (G326 to N330) in another simulation for the *ACE2-K353H* (Figure 7c). In the wild type ACE2, the K353 is a hydrogen donor, and its mutant H353 cannot form the hydrogen bond with the CoV2-RBD as in the wild type CoV2-RBD/ACE2 complex. The number of contacting residue pairs was significantly reduced in the *ACE2-K353H* mutant system. This is in line with the report that K353 is more critical than the other residues, as its hydrophobic neighborhood enables this positively charged residue high selectivity to the RBD [27,28].

bioRxiv preprint doi: https://doi.org/10.1101/2020.03.24.005561; this version posted March 27, 2020. The copyright holder for this preprint (which was not certified by peer review) is the author/funder, who has granted bioRxiv a license to display the preprint in perpetuity. It is made available under aCC-BY-NC-ND 4.0 International license.

The physical interactions between the RBD and the ACE2 were quantified for the simulated structures. We considered the molecular mechanics energy E_{MM} , which is composed of the van der Waals and the electrostatic interactions. Furthermore, the number of residue contacts (*NC*) between (RBD and ACE2) was extracted from simulated structures. Both the E_{MM} and *NC* indicate that the RBD interactions with the ACE2 are comparable for CoV2 and SARS spike proteins (Figure 8). From the simulations, the CoV2-RBD has more close contacts with the ACE2 than the SARS-RBD: the numbers of contacts for CoV2-RBD/ACE2 and SARS-RBD/ACE2 are 32.9 and 30.4 respectively. In terms of interaction energies, CoV2-RBD showed slightly weaker interactions with the ACE2 compared to the SARS-RBD (E_{MM} values are -1017.1 kJ/mol vs. -1133.4 kJ/mol). We would like to point out that the energy E_{MM} is the physical interaction between the RBD and the ACE2, rather than the binding energy, which requires accurately incorporating solvation energy and entropy. Furthermore, the standard deviations of E_{MM} are 70.2 kJ/mol and 65.5 kJ/mol for the two complexes. Therefore, we infer that the binding affinities are comparable for CoV2-RBD/ACE2 and SARS-RBD/ACE2. The simulations started from the predicted and crystal models yielded very similar results (purple triangles). This is in line with a recent study, in which the authors showed similar binding affinity to human ACE2 for both SARS-CoV-2 and SARS-CoV spike proteins [29]. They found the association rate constants k_{on} to be the same at 1.4×10^5 $M^{-1}s^{-1}$, while the SARS-CoV spike protein showed a faster dissociation, with the rate constant k_{off} to be 7.1×10^{-4} s^{-1}, about 4.4 times larger than the SARS-CoV-2 spike protein $k_{off} = 1.6 \times 10^{-4}$ s^{-1}. similar k_{on} values and the equilibrium dissociation constants K_D in nanomolar range were reported in other studies for SARS-CoV-2 spike protein (or RBD) binding to human ACE2[10,30].

More interestingly, the mutation impacts were reflected in the E_{MM} and *NC* analysis: the *ACE2-mut_h1* is likely to reduce the binding to the ACE2 due to the tilting movement of CoV2-RBD, making it further from the ACE2 helix-1 (the blue triangle symbol at lower right, see Figure 7a for the representative structure). In the other simulation trajectory for the CoV2-RBD/ACE2-mut_h1 complex (blue triangle at the left upper corner), the largest *NC* was observed among all simulations. For simulations of the complex with *ACE2-K353H* mutants (green diamonds), the number of contacts were both reduced compared to the wild type system. In one simulation, the contacts between the CoV2-RBD and the

bioRxiv preprint doi: https://doi.org/10.1101/2020.03.24.005561; this version posted March 27, 2020. The copyright holder for this preprint (which was not certified by peer review) is the author/funder, who has granted bioRxiv a license to display the preprint in perpetuity. It is made available under aCC-BY-NC-ND 4.0 International license.

Helix-13 of the ACE2 were completely lost (see Figure 7c), consistent with the less favorable interactions reflected on an increase of E_{MM}. For the SARS-RBD interaction with the *ACE2-mut_h1*, both simulations revealed fewer contacts compared to the wild type SARS-RBD/ACE2 complex (purple stars in Figure 8).

Discussions and Conclusion

The homology modeling of the CoV2-RBD/ACE2 complex yielded highly consistent models compared to the crystal structures. All-atom molecular dynamics simulations were carried out to study the dynamic interactions of CoV2-RBD with human ACE2, the results were compared to the SARS-RBD/ACE2 system. The human ACE2 mutants were also constructed to mimic the rat ACE2 to investigate the roles of critical residues, and possible binding modes in other mammals. It is observed that MD simulations improved the structure at the binding interface and strengthened the interactions between the subunits. The structure of the complex interface is highly stable for all simulations of CoV2-RBD/ACE2 complex in the wild type. The loop region between β6 and β7 can potentially form more contacts with the ACE2 as observed in one simulation trajectory. The simulations results also reveal that the interactions between CoV2-RBD and the ACE2 are mediated by water molecules at the interfaces, stressing the necessity of accounting for the explicit water molecules when quantifying the binding affinity.

The interactions between the RBD and the ACE2 were quantified by physical interaction energies (molecular mechanics energy) and the number of contacting residues. The detailed comparison results suggest that the CoV2-RBD and the SARS-RBD bind to human ACE2 with comparable affinity. The comparison between the SARS-RBD/ACE2 and the CoV2-RBD/ACE2 complexes, with the former forms fewer contacts than the latter (Figure 8), yet exhibiting stronger interactions. The decomposition of the E_{MM} to the van der Waals and the electrostatic interactions revealed that the major difference is attributed to the electrostatic interactions. Furthermore, we compared the major contacting residues and found that the SARS-RBD has two charged residues (R426 and D463) and the CoV2-RBD has only one charged residue (K417) at the complex interface. The polar and hydrophobic residues are comparable in the two RBDs. This is consistent with the statistics of hydrogen bonds at the complex interfaces.

bioRxiv preprint doi: https://doi.org/10.1101/2020.03.24.005561; this version posted March 27, 2020. The copyright holder for this preprint (which was not certified by peer review) is the author/funder, who has granted bioRxiv a license to display the preprint in perpetuity. It is made available under aCC-BY-NC-ND 4.0 International license.

This study was started with a structure predicted using homology modeling method, which later found to be highly consistent with the crystal structure, demonstrating the potentiality of structure prediction and dynamics simulation in revealing molecular details before the availability of high resolution experimental information. Furthermore, the interactions between CoV2-RBD and the ACE2 mutants mimicking rat ACE2 protein were investigated. The results provide valuable information at the atomic level for the reduced binding affinity. The recent report on the SARS-CoV-2 infection to a dog [31] raise the concerns about the COVID-19 transmissions to pet animals. The approach discussed in this study can be applied to analyze the CoV2-RBD interaction with a broader ACE2 variants, including the genetic polymorphism of the ACE2 in human and the ACE2 of other mammalian animals. Preliminary analysis of several ACE2 proteins from mammalian animals using homology modeling and active site prediction methods shows that the binding sites exhibit different features compared to the human ACE2. More systematic and deeper analysis will be carried out using the presented approach.

Acknowledgement

The work is supported by Beijing Computational Science Research Center (CSRC) via a director discretionary grant. The authors acknowledge the Beijing Super Cloud Computing Center (BSCC) for providing HPC resources that have contributed to the research.

Competing interests

The authors declare no competing interests.

bioRxiv preprint doi: https://doi.org/10.1101/2020.03.24.005561; this version posted March 27, 2020. The copyright holder for this preprint (which was not certified by peer review) is the author/funder, who has granted bioRxiv a license to display the preprint in perpetuity. It is made available under aCC-BY-NC-ND 4.0 International license.

Reference:

1. Zhu, N. *et al.* A Novel Coronavirus from Patients with Pneumonia in China, 2019. *N. Engl. J. Med.* NEJMoa2001017 (2020). doi:10.1056/nejmoa2001017
2. Wu, F. *et al.* A new coronavirus associated with human respiratory disease in China. *Nature* (2020). doi:10.1038/s41586-020-2008-3
3. Xu, X. & Chen, P. Evolution of the novel coronavirus from the ongoing Wuhan outbreak and modeling of its spike protein for risk of human transmission. *Sci. CHINA Life Sci.* 1–4 (2020). doi:10.1007/s11427-020-1637-5
4. Lu, R. *et al.* Genomic characterisation and epidemiology of 2019 novel coronavirus: implications for virus origins and receptor binding. *Lancet* **395**, 565–574 (2020).
5. Li, W. *et al.* Angiotensin-converting enzyme 2 is a functional receptor for the SARS coronavirus. *Nature* **426**, 450–454 (2003).
6. Wong, S. K., Li, W., Moore, M. J., Choe, H. & Farzan, M. A 193-Amino Acid Fragment of the SARS Coronavirus S Protein Efficiently Binds Angiotensin-converting Enzyme 2. *J. Biol. Chem.* **279**, 3197–3201 (2004).
7. Li, F., Li, W., Farzan, M. & Harrison, S. C. Structure of SARS coronavirus spike receptor-binding domain complexed with receptor. *Science.* **309**, 1864–1868 (2005).
8. Kuba, K., Imai, Y., Ohto-Nakanishi, T. & Penninger, J. M. Trilogy of ACE2: A peptidase in the renin-angiotensin system, a SARS receptor, and a partner for amino acid transporters. *Pharmacology and Therapeutics* **128**, 119–128 (2010).
9. Bao, L. *et al.* The Pathogenicity of 2019 Novel Coronavirus in hACE2 Transgenic Mice. *bioRxiv* 2020.02.07.939389 (2020). doi:10.1101/2020.02.07.939389
10. Lan, J. *et al.* Crystal structure of the 2019-nCoV spike receptor-binding domain bound with the ACE2 receptor. *bioRxiv* 1–20 (2020). doi:10.1101/2020.02.19.956235
11. Waterhouse, A. *et al.* SWISS-MODEL: Homology modelling of protein structures and complexes. *Nucleic Acids Res.* **46**, W296–W303 (2018).
12. Li, W. *et al.* Efficient Replication of Severe Acute Respiratory Syndrome Coronavirus in Mouse Cells Is Limited by Murine Angiotensin-Converting Enzyme 2. *J. Virol.* **78**, 11429–11433 (2004).
13. Wan, Y., Shang, J., Graham, R., Baric, R. S. & Li, F. Receptor recognition by novel coronavirus from Wuhan: An analysis based on decade-long structural studies of SARS. *J. Virol.* (2020). doi:10.1128/jvi.00127-20
14. Lee, J. *et al.* CHARMM-GUI Input Generator for NAMD, GROMACS, AMBER, OpenMM, and CHARMM/OpenMM Simulations Using the CHARMM36 Additive Force Field. *J. Chem. Theory Comput.* **12**, 405–413 (2016).
15. Best, R. B. *et al.* Optimization of the additive CHARMM all-atom protein force field targeting improved sampling of the backbone φ, ψ and side-chain χ1 and χ2 Dihedral Angles. *J. Chem. Theory Comput.* **8**, 3257–3273 (2012).
16. Nosé, S. A unified formulation of the constant temperature molecular dynamics methods. *J. Chem. Phys.* **81**, 511–519 (1984).
17. Hoover, W. G. Canonical dynamics: Equilibrium phase-space distributions. *Phys. Rev. A* **31**, 1695–1697 (1985).
18. Parrinello, M. & Rahman, A. Polymorphic transitions in single crystals: A new molecular dynamics method. *J. Appl. Phys.* **52**, 7182–7190 (1981).
19. Abraham, M. J. *et al.* Gromacs: High performance molecular simulations through multi-level parallelism from laptops to supercomputers. *SoftwareX* **1**–**2**, 19–25 (2015).
20. Darden, T., York, D. & Pedersen, L. Particle mesh Ewald: An N·log(N) method for Ewald sums in large systems. *J. Chem. Phys.* **98**, 10089–10092 (1993).

bioRxiv preprint doi: https://doi.org/10.1101/2020.03.24.005561; this version posted March 27, 2020. The copyright holder for this preprint (which was not certified by peer review) is the author/funder, who has granted bioRxiv a license to display the preprint in perpetuity. It is made available under aCC-BY-NC-ND 4.0 International license.

21. Hess, B., Bekker, H., Berendsen, H. J. C. & Fraaije, J. G. E. M. LINCS: A Linear Constraint Solver for molecular simulations. *J. Comput. Chem.* **18**, 1463–1472 (1997).
22. Kumari, R., Kumar, R. & Lynn, A. G-mmpbsa -A GROMACS tool for high-throughput MM-PBSA calculations. *J. Chem. Inf. Model.* **54**, 1951–1962 (2014).
23. Humphrey, W., Dalke, A. & Schulten, K. VMD: Visual molecular dynamics. *J. Mol. Graph.* **14**, 33–38 (1996).
24. Pettersen, E. F. *et al.* UCSF Chimera - A visualization system for exploratory research and analysis. *J. Comput. Chem.* **25**, 1605–1612 (2004).
25. Li, W. *et al.* Receptor and viral determinants of SARS-coronavirus adaptation to human ACE2. *EMBO J.* **24**, 1634–1643 (2005).
26. Lavillette, D. *et al.* Significant redox insensitivity of the functions of the SARS-CoV spike glycoprotein: Comparison with HIV envelope. *J. Biol. Chem.* **281**, 9200–9204 (2006).
27. Li, F. Structural analysis of major species barriers between humans and palm civets for severe acute respiratory syndrome coronavirus infections. *J. Virol.* **82**, 6984–6991 (2008).
28. Li, F. Receptor Recognition Mechanisms of Coronaviruses: a Decade of Structural Studies. *J. Virol.* **89**, 1954–1964 (2015).
29. Walls, A. C. *et al.* Structure, Function, and Antigenicity of the SARS-CoV-2 Spike Glycoprotein. *Cell* **0**, (2020).
30. Wrapp, D. *et al.* Cryo-EM structure of the 2019-nCoV spike in the prefusion conformation. *Science (80-.).* **367**, 1260–1263 (2020).
31. Coronavirus: Hong Kong confirms a second dog is infected. (2020). Available at: https://www.scmp.com/news/hong-kong/health-environment/article/3075993/coronavirus-hong-kong-confirms-second-dog.

bioRxiv preprint doi: https://doi.org/10.1101/2020.03.24.005561; this version posted March 27, 2020. The copyright holder for this preprint (which was not certified by peer review) is the author/funder, who has granted bioRxiv a license to display the preprint in perpetuity. It is made available under aCC-BY-NC-ND 4.0 International license.

Figure Legends

Figure 1. The predicted structure and the binding interface. (**a**) Predicted model of the CoV2-RBD/ACE2; (**b**) Crystal structure of the SARS-RBD/ACE2 (PDB: 2AJF); (**c**) Superposed models. The binding interface is indicated in the boxed region.

Figure 2. Representative structures extracted from simulation trajectories using clustering analysis. (**a**) The most populated structure from simulation trajectory#1, with the loop (L_{67}, S477-G485) between β6 and β7 moved towards the ACE2 helix-1, forming additional contacts. (**b, c**) The most populated structures in the simulations #2 and #3. The complex structures and the binding interfaces are similar to the predicted model and the crystal structure. (**d**) The comparison of initial (cyan) and representative (pink) structures to the crystal structure (gold) of CoV2-RBD/ACE2. The side chain of K31 (encircled in the red boxes) was refined to the correct position during the MD simulations (right panel).

Figure 3. The dynamics analysis of the simulation trajectory. (**a**) The root-mean-square-deviation (RMSD) of the simulated structures compared to the initial and representative models. (**b**) The residue level fluctuations of CoV2-RBD in three simulations. The shaded area corresponds to the CoV2-RBD binding region to the ACE2.

Figure 4. The collective motion of the CoV2-RBD/ACE2 complex. (a) The representative model (blue) from wild type CoV2-RBD/ACE2 simulations superposed to the initial model (silver). The arrows indicate the directions of the collective motion, and the hinge region is colored in red. **(b)** The same representation for the CoV2-RBD complexed with the ACE2 h1-mut mutant (green), and comparison between the initial model (silver) and the representative model (green) indicates a large tilting movement compared to the wild type system.

Figure 5. The hydrogen bonds between the CoV2-RBD and the ACE2. (**a**) The number of hydrogen bonds extracted from the simulation data using Donor-Receptor distance cutoff of 3.0 Å. (**b**) Same as (a) except that the cutoff distance was relaxed to 3.9 Å. The trend lines were obtained by least square fitting.

bioRxiv preprint doi: https://doi.org/10.1101/2020.03.24.005561; this version posted March 27, 2020. The copyright holder for this preprint (which was not certified by peer review) is the author/funder, who has granted bioRxiv a license to display the preprint in perpetuity. It is made available under aCC-BY-NC-ND 4.0 International license.

Figure 6. The water molecules at the binding interface. (**a**) The number of water molecules that bridge the CoV2-RBD and ACE2 found in a simulation trajectory. (**b**) The water molecules at the interface for the initial structure after equilibration. (**c**) The water molecules at the interface as observed in the crystal structure.

Figure 7. The representative structures for the ACE2-mutants in complex with the CoV2-RBD. (**a**, **b**) *ACE2-mut-h1*, in which the human ACE2 helix-1 (residues 19-40) was mutated to the Rat sequence. The structure in (a) is the same as the green model shown in Figure 4b, which illustrates a pronounced tilting movement. (**c**, **d**) *ACE2-K353H*, where the ACE2 K353 was mutated to a histidine. The CoV2-RBD in (c) lost its contact with the Helix-13 of the ACE2 (residues 498-503, indicated by the black arrow). Each structure was obtained by the clustering analysis of 500ns MD simulation trajectories.

Figure 8. The interaction energies and the residue contacts between the RBD and the ACE2. The molecular mechanics interactions and the number of contacting residue pairs were obtained from the structures sampled by MD simulations. In the legend, the CoV2 and SARS indicate the sources of the RBD; the WT, K353H, mut_h1 are the abbreviations for different constructs of the human ACE2, corresponding to the wild type, the mut_h1, and the K353H.

bioRxiv preprint doi: https://doi.org/10.1101/2020.03.24.005561; this version posted March 27, 2020. The copyright holder for this preprint (which was not certified by peer review) is the author/funder, who has granted bioRxiv a license to display the preprint in perpetuity. It is made available under aCC-BY-NC-ND 4.0 International license.

Table 1. The ACE2 mutants to mimic the Rat ACE2.

Mutant name	Mutations on ACE2	Remark
mut_h1	T20L, Q24K, K26E, T27S, D30N, H34Q, F40S	L20, N30, Q34, and S40 are conserved between rat and mouse.
K353H	K353H	H353 is conserved between rat and mouse

Table 2. Contact residues between the CoV2-RBD and the ACE2.
Green color denotes new interaction not observed in crystal structure.

Model#1		Model#2		Model#3	
ACE2	*CoV*	*ACE2*	*CoV*	*ACE2*	*CoV*
Q24	K417	S19	K417	Q24	K417
T27	Y453	Q24	G446	T27	G446
F28	L455	T27	Y449	F28	Y449
D30	F456	F28	Y453	D30	Y453
K31	Q474	D30	L455	K31	L455
H34	A475	K31	F456	H34	F456
E35	G476	H34	A475	E35	A475
E37	S477	E35	F486	E37	F486
D38	T478	D38	N487	D38	N487
Y41	G485	Y41	Y489	Y41	Y489
Q42	F486	Q42	Q493	Q42	Q493
M82	N487	L45	Y495	M82	Y495
Y83	Y489	M82	G496	Y83	G496
N330	Q493	Y83	Q498	N330	Q498
K353	Y495	N330	T500	K353	T500
G354	G496	K353	N501	G354	N501
D355	Q498	G354	G502	D355	G502
R357	T500	D355	Y505	R357	Y505
	N501	R357			
	G502				
	Y505				

bioRxiv preprint doi: https://doi.org/10.1101/2020.03.24.005561; this version posted March 27, 2020. The copyright holder for this preprint (which was not certified by peer review) is the author/funder, who has granted bioRxiv a license to display the preprint in perpetuity. It is made available under aCC-BY-NC-ND 4.0 International license.

Table S1. Contact residues at the SARS-COV- RBD/ACE2 interface

Traj 1		Traj2		Traj 3	
ACE2	*CoV*	*ACE2*	*CoV*	*ACE2*	*CoV*
S19	R426	Q24	R426	Q24	R426
Q24	Y436	T27	Y436	T27	Y440
T27	Y440	D30	Y440	K31	Y442
K31	Y442	K31	Y442	H34	L443
H34	L443	H34	L443	E37	P462
E37	D463	E37	P462	D38	D463
D38	L472	D38	D463	Y41	G464
Y41	N473	Y41	G464	Q42	P470
Q42	Y475	Q42	L472	L45L	L472
L45L	N479	L45L	N473	L79L	N473
L79L	G482	L79L	Y475	M82	Y475
M82	Y484	M82	N479	Y83	L478
Y83	T486	Y83	G482	Q325	N479
Q325	T487	Q325	Y484	E329	G482
E329	G488	E329	T486	N330	Y484
N330	I489	N330	T487	K353	T486
K353	Y491	K353	G488	G354	T487
G354		G354	I489	D355	G488
D355		D355	Y491	R357	I489
R357		R357			Y491

Fig.1

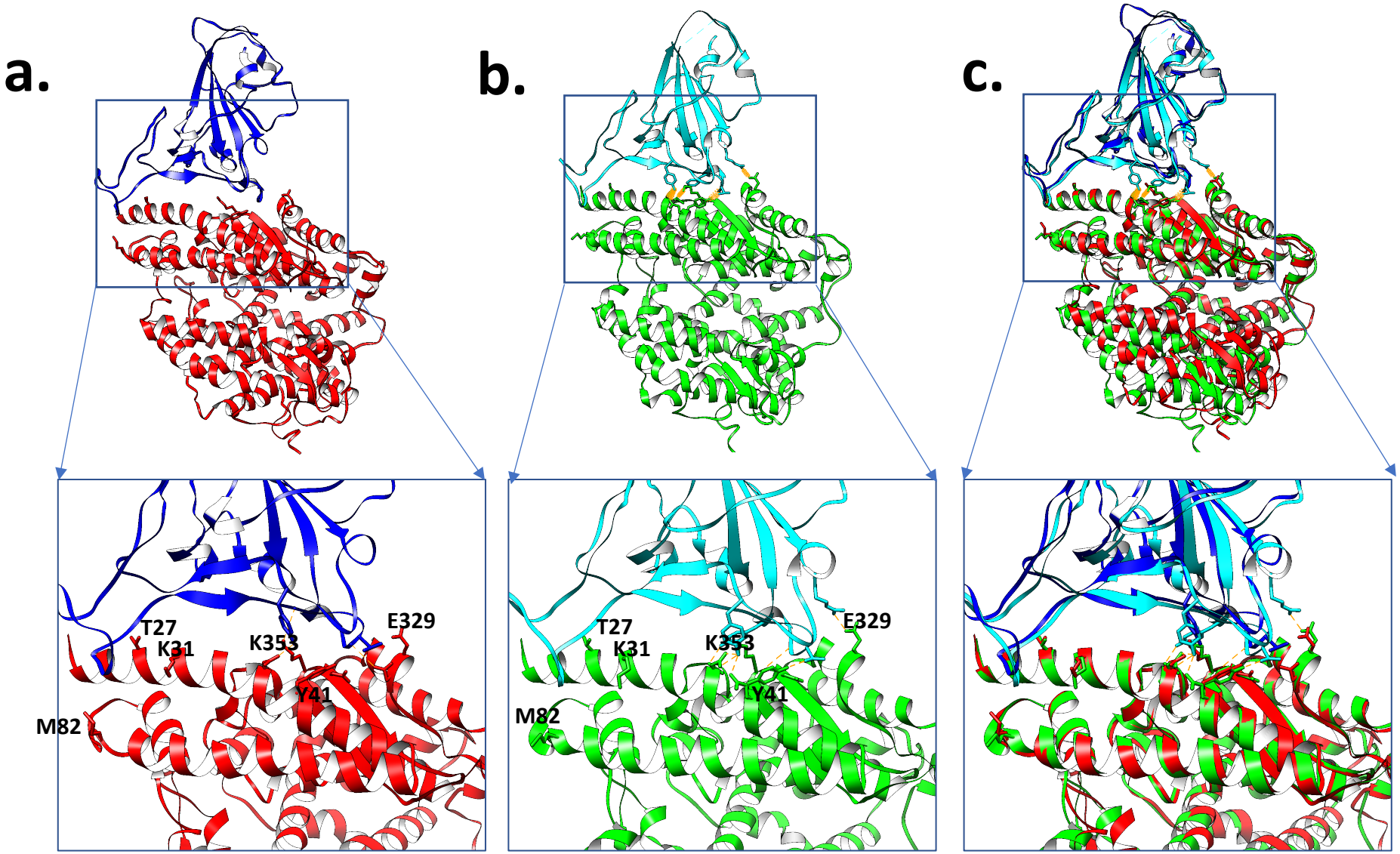

CoV2-RBD/ACE2 SARS-RBD/ACE2 Superposed

Fig.2

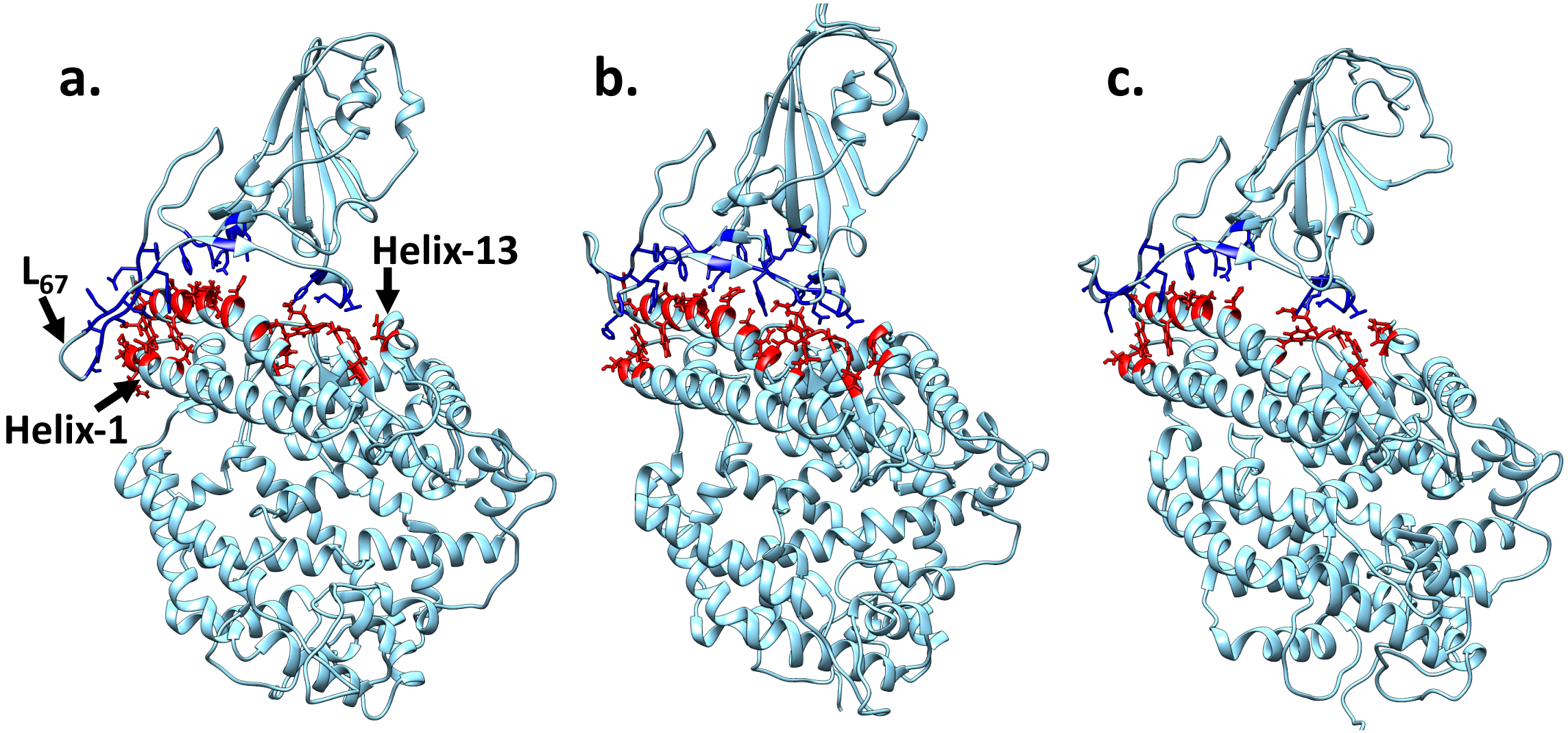

Fig.2

d.

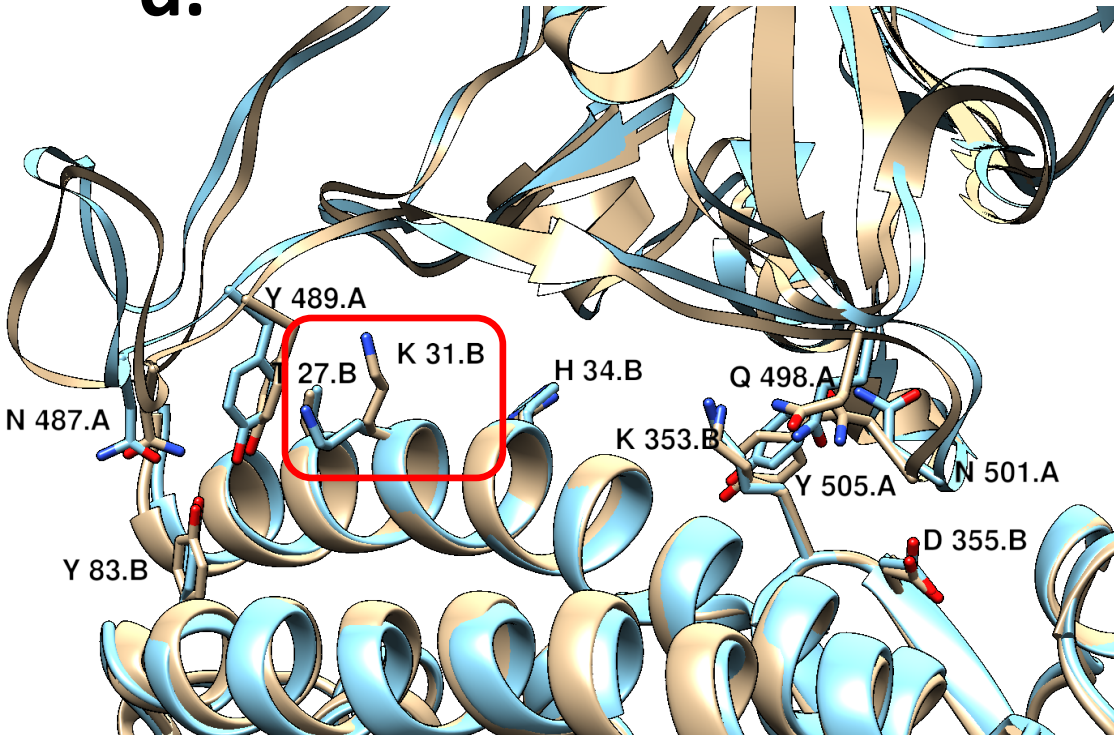
Y 489.A
T 27.B
K 31.B
H 34.B
Q 498.A
N 487.A
K 353.B
Y 505.A
N 501.A
D 355.B
Y 83.B

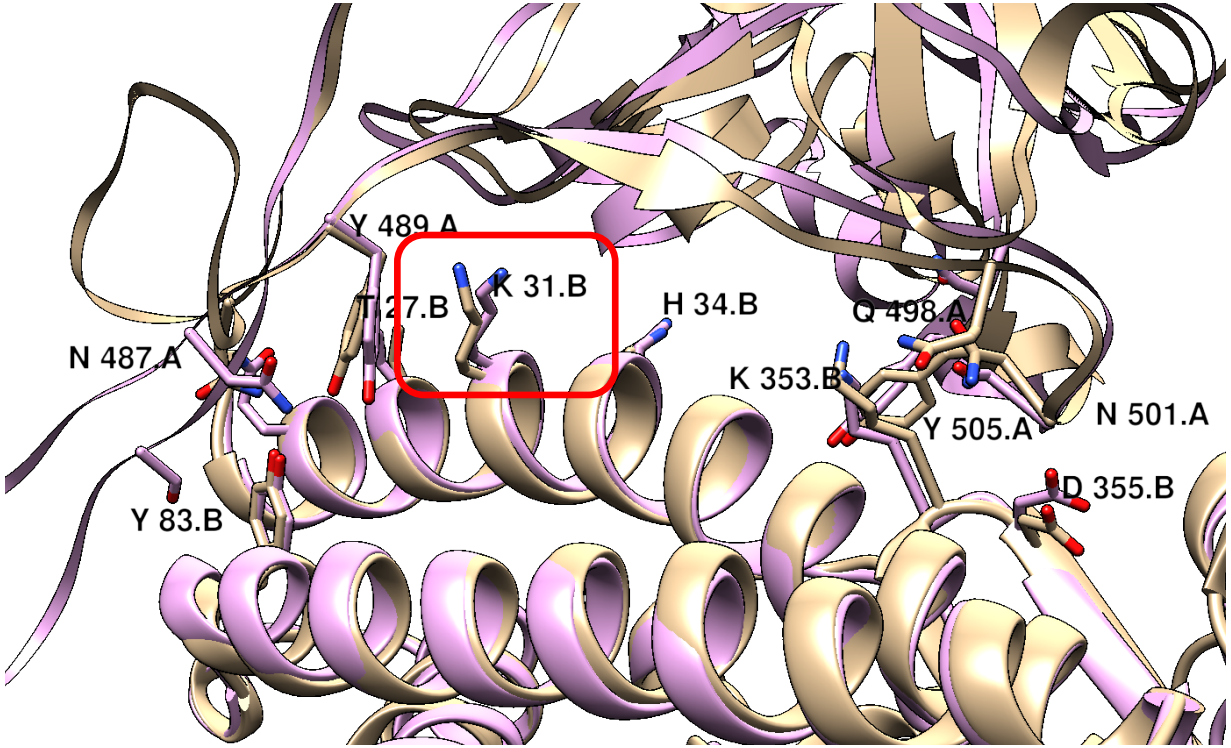
Y 489.A
T 27.B
K 31.B
H 34.B
Q 498.A
N 487.A
K 353.B
Y 505.A
N 501.A
D 355.B
Y 83.B

Fig.3

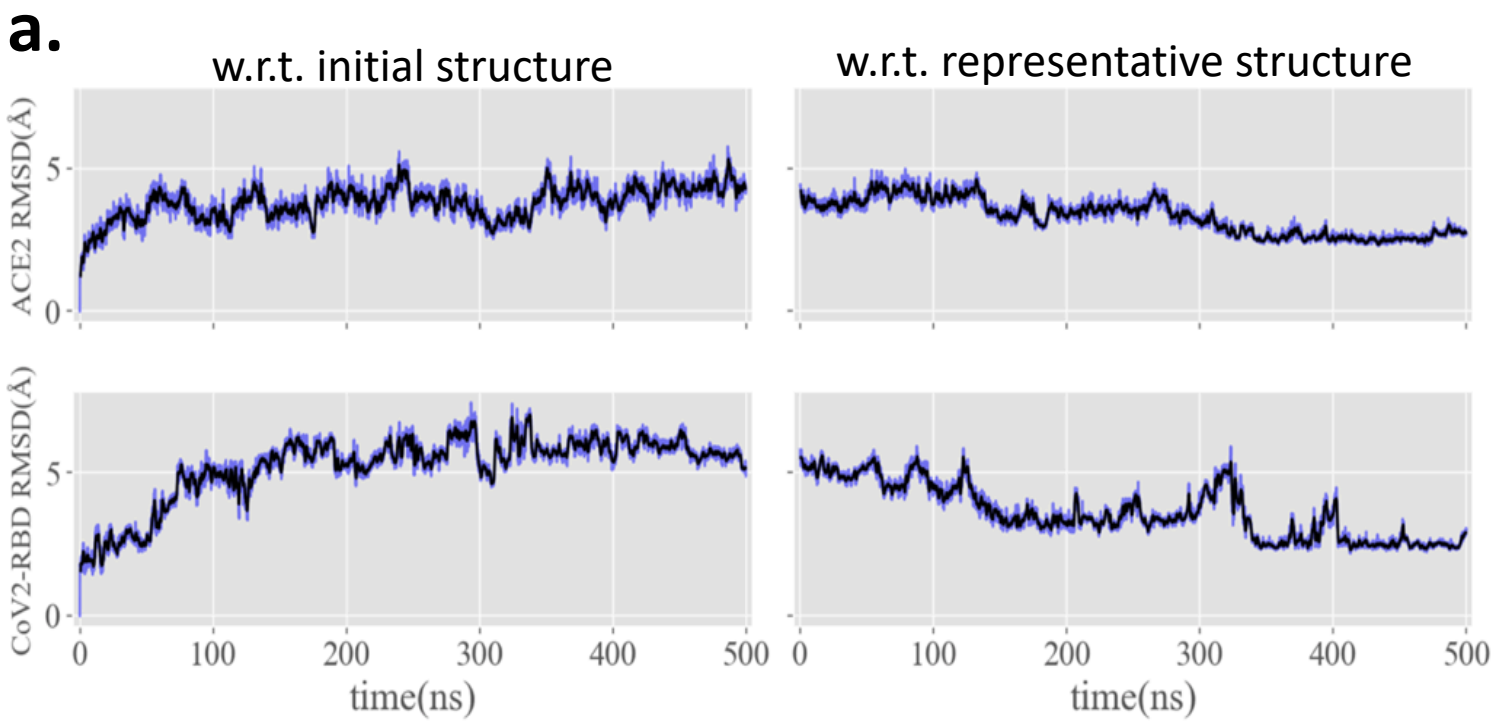
a.
w.r.t. initial structure
w.r.t. representative structure
ACE2 RMSD(Å)
CoV2-RBD RMSD(Å)
0
5
0
100
200
300
400
500
time(ns)

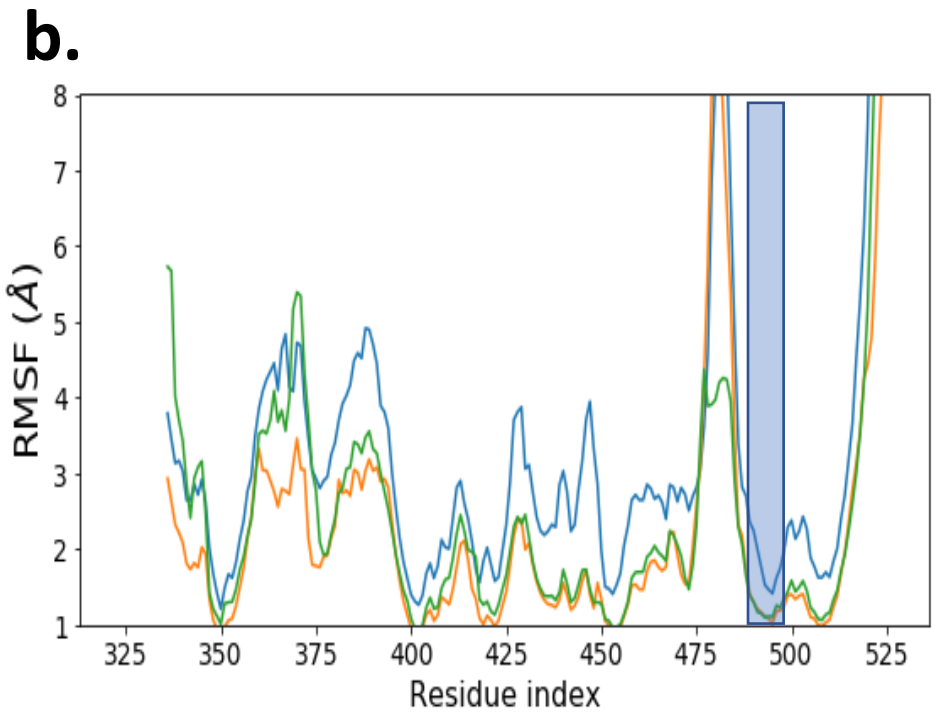
b.
RMSF (Å)
1
2
3
4
5
6
7
8
325
350
375
400
425
450
475
500
525
Residue index

Fig.4

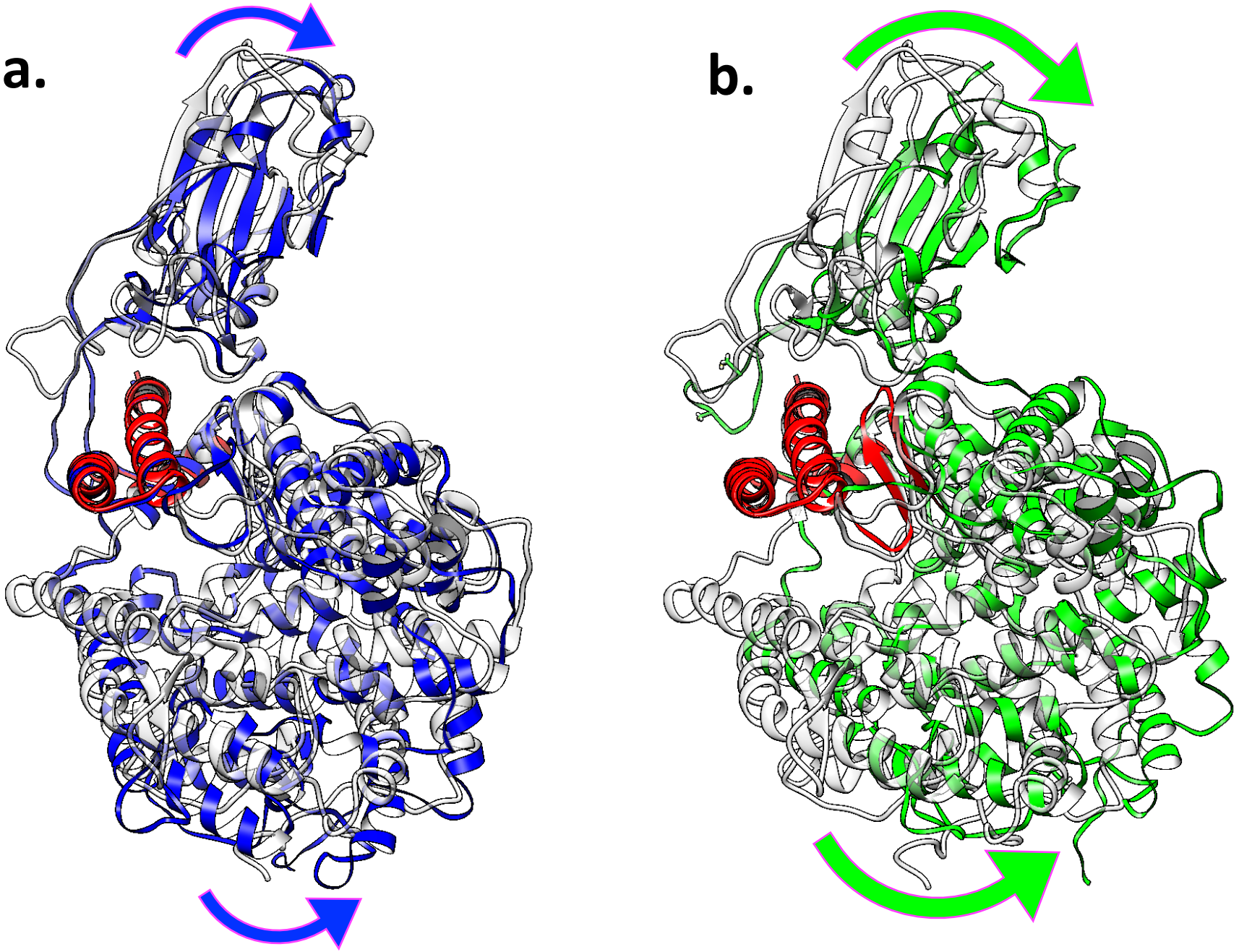

Fig.5

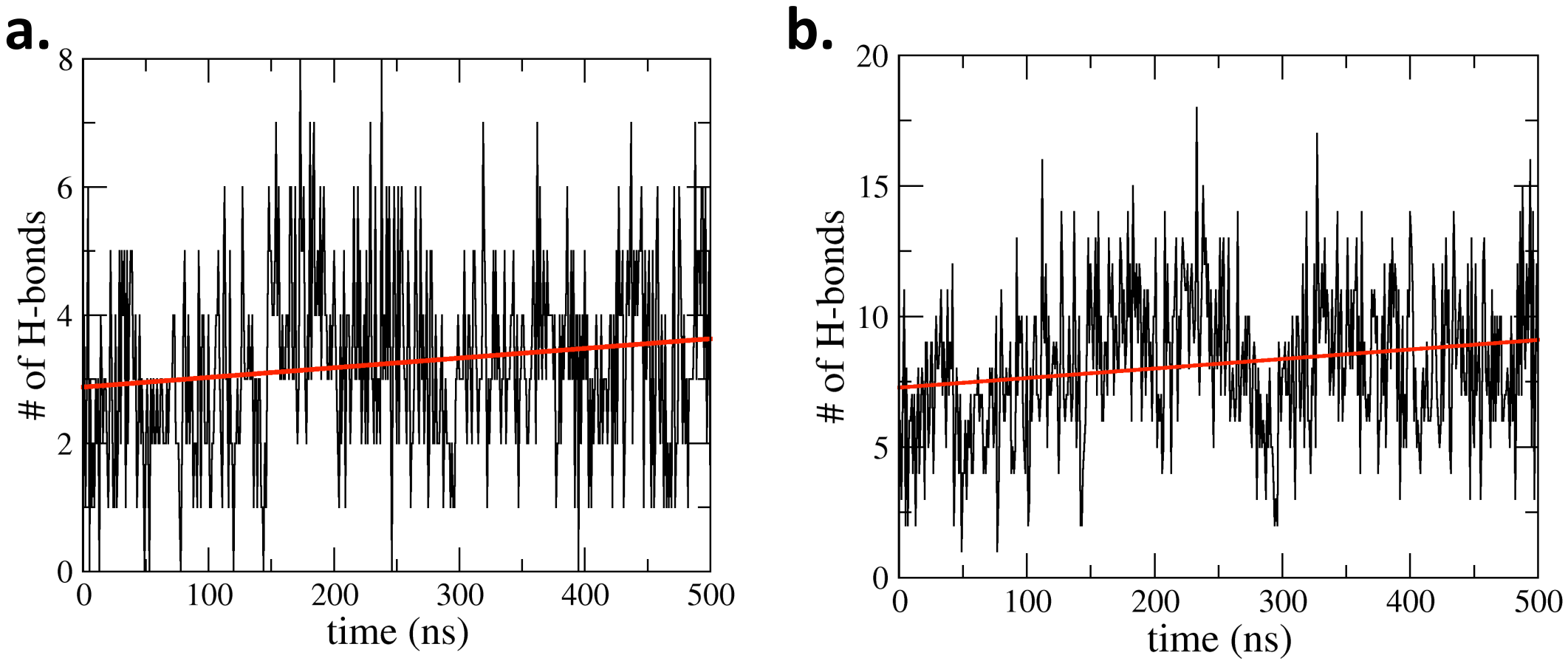
a.
# of H-bonds
time (ns)
0
2
4
6
8
0
100
200
300
400
500
b.
# of H-bonds
time (ns)
0
5
10
15
20
0
100
200
300
400
500

Fig.6

a.

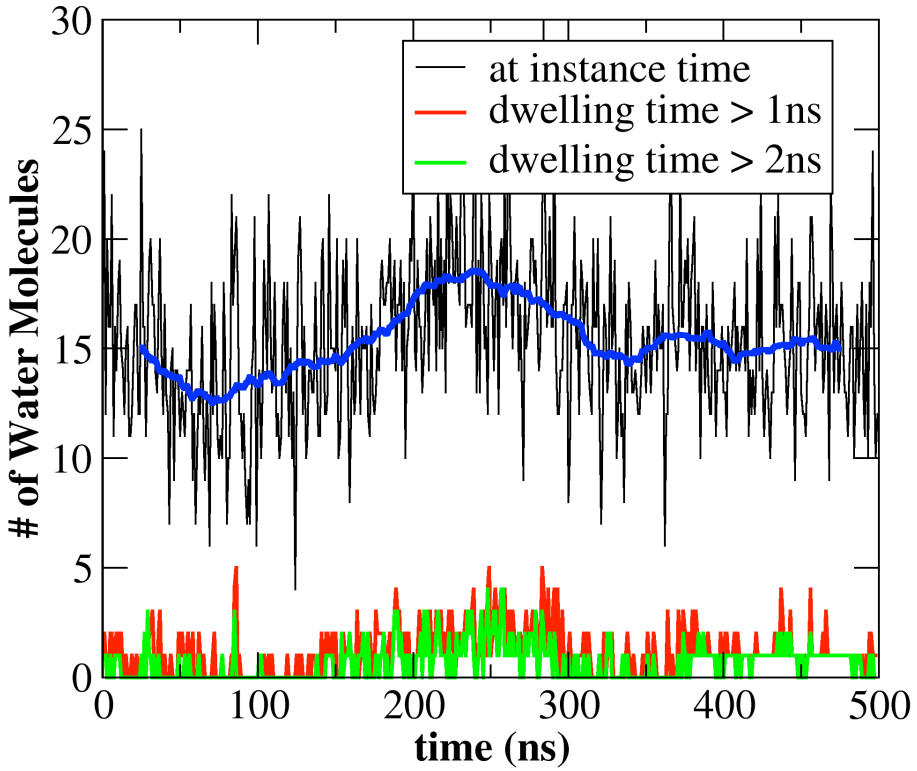
at instance time
dwelling time > 1ns
dwelling time > 2ns
# of Water Molecules
time (ns)
0
5
10
15
20
25
30
0
100
200
300
400
500

b.

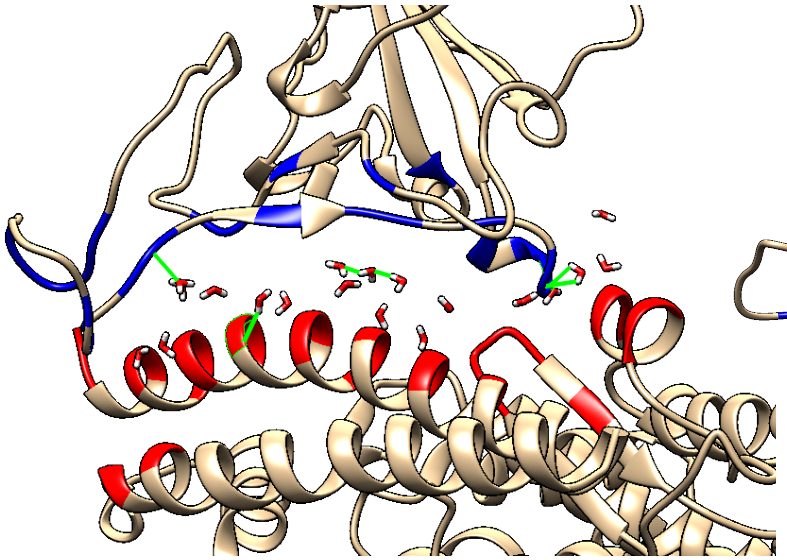

c.

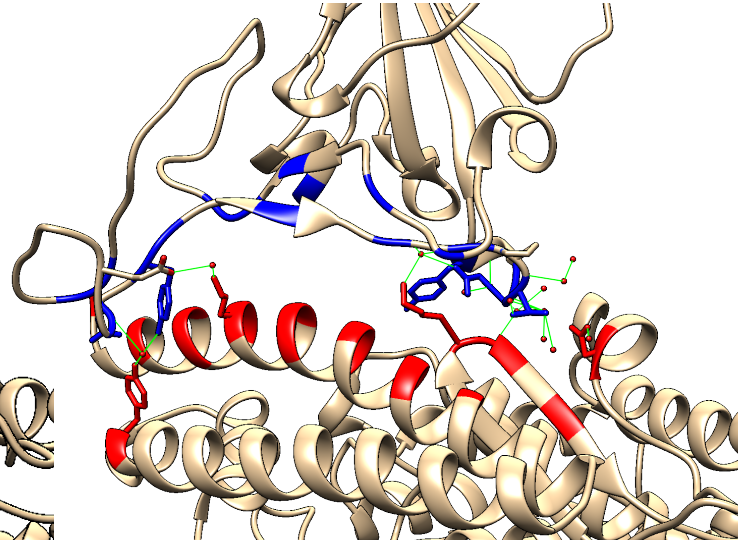

Fig.7

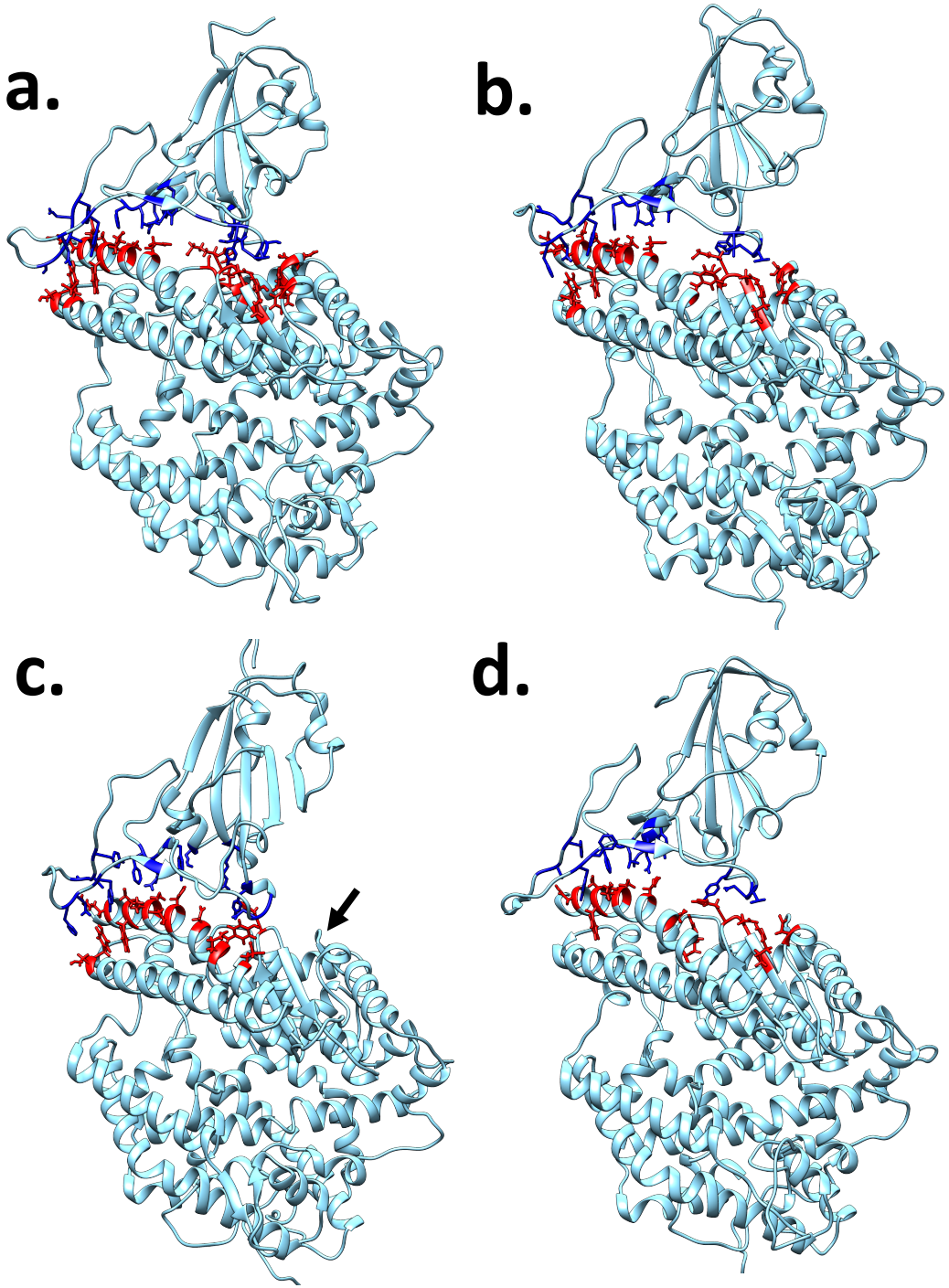

Fig.8

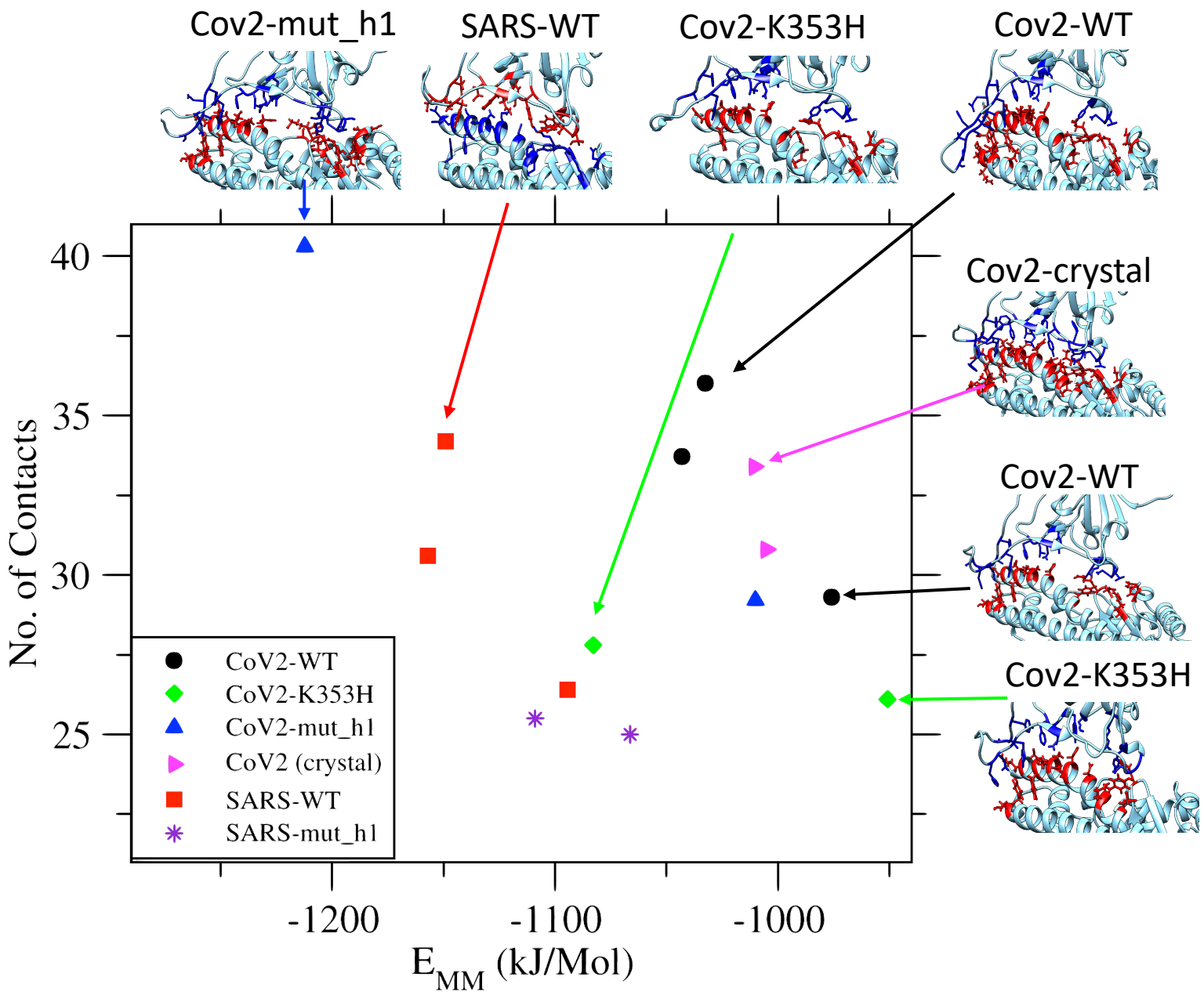
Cov2-mut_h1
SARS-WT
Cov2-K353H
Cov2-WT
Cov2-crystal
Cov2-WT
Cov2-K353H
40
35
30
25
No. of Contacts
-1200
-1100
-1000
E_MM (kJ/Mol)
CoV2-WT
CoV2-K353H
CoV2-mut_h1
CoV2 (crystal)
SARS-WT
SARS-mut_h1